

Numerical Simulation of Hydrodynamic Instability in a Rotating Protoneutron Star by Supernova Explosion II Type

S. D. Ustyugov

KIAM, Moscow, 125047, Russia

Large-scale convective instability owing to the neutronization of matter in a protoneutron star during the collapse of star with low initial entropy are considered. The 3D hydrodynamic calculation on nested grids with three level shows that large-scale bubbles of hot matter with size 10^6 cm arise to surface neutrinosphere. When the bubbles reaches low density, the neutrinos contained in matter freely escape from it in the regime of volume radiation. The characteristic time of this process is equalled to 3.5 ms. The shock from the initial bounce when the collapse in the stellar core stops will then be supported by the neutrino emission, resulting in the ejection of an envelope. In rotating protoneutron star the large scale bubbles come to the surface of the stellar core along the axis of rotation. Neutrino with energy 30-50 MeV are contained in the bubbles. Calculations shows that time of neutrino emission from such bubble is equal near 1 ms with mean energy of neutrino 30-40 MeV.

1. INTRODUCTION

At the present time two mechanisms have been proposed to explain the supernova. The first is connected with the rapid ejection of the stellar envelope when the shock wave (resulting from the rapid compression and deceleration of material at higher-than-nuclear densities) passes through it [1]. The second mechanism involves heating of material behind the shock front by neutrinos, which escape from the neutrinosphere surrounding the protoneutron star and facilitate the further passage of the shock and ejection of the stellar envelope [2]. However, subsequent numerical simulations showed that these two mechanisms are inadequate for several reasons. In the first model, the so-called "fast" mechanism, the shock loses some of its energy during the division of iron-group nuclei into free nucleons; then, when it arrives at the neutrinosphere, the emission of neutrinos from the front carries away energy and decreases the lepton number in the shock material, decreasing the shock's energy and pressure. All these processes weaken the shock, so that it is stopped in the flow of material accreting around the core [1]. In many ways, the action of the second mechanism is determined by conditions in the region between the neutrinosphere and shock, and is critical for the neutrino luminosity and the mean spectral energy. The required luminosity can be reached only if convection is invoked in both the lower neutrinosphere and at higher levels. In turn, this convection can develop only when the heating of material and formation of a region of instability near the neutrinosphere occurs more rapidly than the motion of material from the shock toward the surface of the protoneutron star [3].

Numerical simulations of convection near and below the neutrinosphere [4] taking into account neutrino transport showed that the convective rate is too small relative to the rate at which material flows in through the boundary of the neutrinosphere to provide a significant transport of energy and leptons. During the

collapse of the iron core, about 99% of the gravitational energy of the forming neutron star is carried away in the form of neutrinos. In order to eject the stellar envelope, some fraction of this energy must be transferred to the outer layers of the star by some efficient and rapid mechanism. Though convection both inside and outside the neutrinosphere can increase the transport of energy to the shock front, certain conditions are necessary for the convection to be realized. For example, the characteristic time for the development of convection should be less than the characteristic times for accretion and neutrino transport. In addition, convection requires constant feeding, similar to the case of entropy convection inside the protoneutron star.

2. NEW MECHANISM OF SUPERNOVAE EXPLOSION

2.1. Formulation

A more realistic mechanism could be associated with the action of large-scale hydrodynamical instabilities; these are due, for example, to rotation or the magnetic field, are manifest at small characteristic times (of order $10^{-3} - 10^{-1}$ s), and can provide the powerful ejection of a flux of neutrino radiation. It was shown in [5] that, as a result of the evolution of the supernova precursor, a rapidly rotating protoneutron star forms, which subsequently separates into two components due to instabilities, forming a close binary. Of course, this process is accompanied by the release of a large number of neutrinos that were initially bound within the protoneutron star [6]. In the magneto-rotational supernova-explosion mechanism proposed in [7] [8], the energy of the shock wave is provided by rotational energy extracted via twisting of the magnetic lines of force.

There is another interesting possible mechanism for the powerful ejection of neutrino radiation [9], asso-

ciated with hydrodynamical motions in the protoneutron star. This model is essentially based on the pioneering work [10] that considers the development of convective instability in a gravitating gaseous sphere (star). The main idea is based on the similarity of the time evolution of meridional cross sections of isentropic surfaces and of normal cross sections of magnetic surfaces during the development of helical MHD instability in a plasma cylinder [11]. As in the case of plasma instability, it was found that large-scale inhomogeneities grow most rapidly. Chandrasekhar and Lebovitz came to the similar conclusion by investigation of convective instability of gaseous masses in a star [12]. It is interesting that such large-scale instabilities have been observed in experiments on controlled nuclear fusion. Analytical estimates and calculations for the two-dimensional problem indicated that the hot inner layers are carried toward the stellar surface on a time scale $\tau \sim R/v_{sound}$.

Three-dimensional calculations of the development of hydrodynamical instability in a protoneutron star with an excess central entropy were carried out in [9]. Large-scale entropy inhomogeneities developed over 4 *ms*, and then moved away from the central region of the star, whose characteristic size is ~ 20 *km*, generating a formation reminiscent of the mushroom cloud of a nuclear explosion in the Earth's atmosphere. The characteristic time for the motion of a single such bubble toward the surface of the protoneutron star is 1 *ms*, providing a mean velocity of $c/150$. Six bubbles with masses of $10^{-2}M_{\odot}$ each rose symmetrically from the center along perpendiculars to the edges of a cube. The intensity of the neutrino radiation during this ejection was 5×10^{52} *erg/s*. The fraction of energy absorbed per gram of matter in the shock extending from the neutrino emission was 2.3×10^{24} *erg g⁻¹ s⁻¹*, which is comparable to the neutrino losses from the shock front. It is important to note, that process of nonequilibrium neutronization leads to occurrence of neutrino with high average energy 80-150 MeV. Our calculation shown, that means emission neutrino is equal 50-80 Mev. These estimates of the energy of the neutrino emission arriving at the shock wave front as the bubble rise toward the neutrinosphere suggest that large-scale convection is capable of supporting a diverging shock wave, leading to the ejection of the supernova envelope.

2.2. Initial state of the problem and numerical technique

When calculating the distributions of density and temperature inside the protoneutron star, we took the central density and temperature to be $\rho_c = 2 \times 10^{14}$ *g/cm³* and $T_c = 10^{11}$ *K*. We applied the equation of state from [13], in the form of a tabulated dependence of the pressure on density and entropy. We

specified the relative number density of electrons to be constant and equal to 0.35. We specified a Gaussian excess entropy distribution at the initial time near the center ($\rho_0 = 0$), $S = S_0 + (S' - S_0) \exp\{-(\mathbf{r} - \mathbf{r}_0)^2/b^2\}$, assumed to be due to some nonequilibrium process. We determined the initial entropy S_0 from the central temperature and density to be $1.6327 k_B/nucleon$. The maximum entropy in the center $S' = 2.8$, and the parameter $b = 0.02$ was chosen such that the size of the region of the entropy perturbation was one-fifth of the total size of the computational region.

The hydrodynamical equations that we used to model processes inside the protoneutron star in the three-dimensional case have the form

$$\rho \frac{d\mathbf{v}}{dt} = -gradP - \frac{\rho GM}{r^3} \mathbf{r}, \quad (1)$$

$$\frac{d\rho}{dt} + \rho div \mathbf{v} = 0, \quad (2)$$

$$\frac{dS}{dt} = 0. \quad (3)$$

Here, ρ is density, \mathbf{v} the velocity of the matter, P pressure and S entropy.

The hydrodynamic equations was written in conservative form

$$\frac{\partial \vec{U}}{\partial t} + \frac{\partial \vec{F}}{\partial x} + \frac{\partial \vec{G}}{\partial y} + \frac{\partial \vec{H}}{\partial z} = \vec{S}$$

The numerical method which we used was an explicit Godunov-type conservative TVD difference scheme with second order by space and time

$$U_{i,j,k}^{n+1} = U_{i,j,k}^n - \Delta t (L(U_{i,j,k}^n) + S_{i,j,k}),$$

where $\Delta t = t^{n+1} - t^n$ and L (in one direction) is

$$L(U_{i,j,k}) = \frac{\tilde{F}_{i+1/2,j,k} - \tilde{F}_{i-1/2,j,k}}{\Delta x_i}$$

Fluxes along each direction, for example x , was defined by local-characteristic method [14] as follows

$$\tilde{F}_{i+1/2,j,k} = \frac{1}{2} [F_{i,j,k} + F_{i+1,j,k} + R_{i+1/2} W_{i+1/2}]$$

The one step of time integration is defined by Runge-Kutta method [15].

For higher resolution in the numerical modelling we have used three level of nested rectangular grids with 128 cells in each directions. Solution results for above described problem were obtained due to the NORMA system application [16] on the system with distributed memory multiprocesseres (two Alpha 21264/667 MHz in node, memory 1 Gb in node, SAN Myrinet to communication, 384 nodes). Norma program was compiled in Fortran with MPI library. The speedup of computation in 122.8 times on 128 processors were obtained during solution process.

2.3. Results of hydrodynamical simulation.

At the initial time, we obtained an equilibrium configuration allowing for the star's rotation using the iterative method presented in [17]. modified for an arbitrary equation of state. We performed calculations for two cases. The first had no rotation, which we used to test the resulting equilibrium of the star. The second had slow, rigid-body rotation, with the ratio of the rotational kinetic energy T and the gravitational energy $|W|$ chosen to be $T/|W| = 0.01$. We calculated the kinetic and potential energies for integrated quantities derived using the density profile obtained in the computations. The rotational period of the star, which corresponds to the ratio of the kinetic and potential energies, 1%, was $14ms$. We chose the coordinate system such that the plane of rotation coincided with the Oxy axis. This means that the angular-rotation vector of the star has only one component, $\Omega_z = \Omega = const$.

Results of hydrodynamics modelling are shown in Fig.1. In contrast to the models considered in [9] [18], here, two bubbles form after $\sim 3ms$, and become elongated in opposite directions along the rotation axis. Four additional bubbles arise slightly later, after $\sim 5ms$, in the plane of rotation of the protoneutron star. This entropy distribution disrupts the symmetry of the picture obtained in [18]. The bubbles on the rotation axis are the first to tear away from the hot core and float up toward the surface. This occurs because the density changes more rapidly along the rotation axis. Cooler material sinks toward the center of the protoneutron star in the space between these two bubbles. The bubbles in the plane of rotation break away form the hot core somewhat later, and also rise toward the surface. Our computations indicate that, after the first bubbles, additional smaller bubbles form, and also begin to float toward the surface.

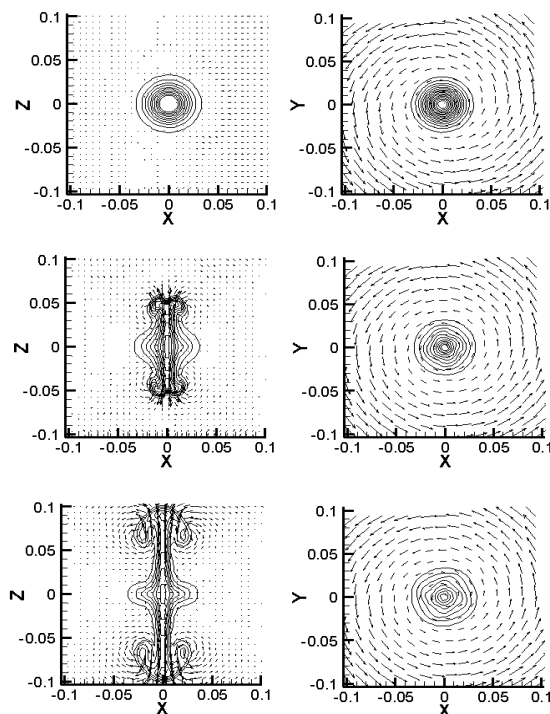


Figure 1: Levels of entropy and fields of velocity in meridional and equatorial planes are shown.

3. NEUTRINO TRANSPORT

3.1. Formulation

Consider a bubble corresponding to a bounded region in the central part of a star about $6 \times 10^5 cm$ in size, with a density of about $2 \times 10^{14} g/cm^3$ and adopt the time dependence for the bubble density obtained from numerical simulation. We assume that, at the initial time, the bubble is composed of iron nuclei ($A = 56, Z = 26$) and free ultrarelativistic electrons. Neutrino interact with matter via both direct and inverse beta processes and elastic interactions with electrons and nuclei.

We emphasize that, due to the large difference between the masses of electrons and nuclei, neutrinos lose substantially greater energy in collisions with electrons. Since our treatment will be limited to a uniform and isotropic approximation for the neutrino distribution function (whereas scattering by nuclei contributes appreciably only to the anisotropic component of the distribution function), we can neglect scattering by nuclei in the collision integral. However, since scattering by nuclei appreciably affects the rate of escape of neutrinos through the bubble boundary, we will take it into account in this process. We neglect all other processes involving neutrinos. In contrast to [19], we shall take into account the fact that there is also some distribution of neutrinos outside

the bubble. Therefore, neutrinos can both leave and enter the region under consideration. The electron distribution function will be interpolated by a Fermi step function, which is obviously applicable only when $E_F \gg 1.5kT$ (i.e., when the Fermi energy of the electrons is considerably greater than their thermal energy).

3.2. Mathematical model

In a uniform, isotropic approximation, the kinetic equation describing the evolution of the neutrino distribution in a bounded region whose characteristic size d , density, and partial concentrations of components vary with time can be written in the form

$$\begin{aligned} \frac{\partial f(p, t)}{\partial t} = & 4\pi \left[(1 - f(p, t)) \int_0^\infty dp' (p')^2 f(p', t) K^{in}(p, p', t) - \right. \\ & \left. f(p, t) \int_0^\infty dp' (p')^2 (1 - f(p', t)) K^{out}(p, p', t) \right] + \\ & \frac{d\rho(t)}{\rho(t)dt} f(p, t) - \frac{c}{d(t)[1 + \gamma(p, t)]} (f(p, t) - f_g(p, p_g)) + \\ & (1 - f(p, t))S(p, t) - f(p, t)Y(p, t). \quad (4) \end{aligned}$$

Here, the functions $K^{in}(p, p', t)$ and $K^{out}(p, p', t)$ depend on details of the process of neutrino scattering by electrons, and $S(p, t)$ and $Y(p, t)$ are sources and sinks of neutrinos, determined by the direct and inverse beta processes. The term containing the logarithmic derivative of the density is responsible for variations in the neutrino distribution due to the changing dimensions of the region where the neutrinos are concentrated. The last term describes neutrino escape through the boundary. (The value $\gamma = 0$ corresponds to the case of free propagation.) We normalized the distribution function as follows:

$$n(t) = 4\pi(2\pi\hbar)^{-3} \int_0^\infty dp' (p')^2 f(p', t). \quad (5)$$

This equation for the neutrino distribution function must be supplemented by an equation describing evolution of the electron number density

$$\begin{aligned} \frac{dn_e(t)}{dt} = & 4\pi \int_0^\infty dp p^2 [-(1 - f(p, t))S(p, t) + f(p, t)Y(p, t)] \\ & + \frac{d\rho}{\rho dt} n_e(t), \quad (6) \end{aligned}$$

and also by a relation between the densities of the electrons and neutrons, on the one hand, and the density of the medium, on the other:

$$m_n \left[n_n(t) + \frac{A}{Z} n_e(t) \right] = \rho(t). \quad (7)$$

In deriving (7), we have assumed that electrons make a negligible contribution to the density of the medium, and that the medium is electrically neutral.

We used the following expressions for γ in the simulations:

$$\begin{aligned} \gamma(x, t) = & 4\pi \int_0^\infty dy y^2 (1 - f(y, t)) [K^{out}(x, y, t) + K^{in}(x, y, t)], \quad (8) \end{aligned}$$

and

$$\begin{aligned} \gamma(x, t) = & 4\pi \int_0^\infty dy y^2 [(1 - f(y, t))K^{out}(x, y, t) + K^{in}(x, y, t)]. \quad (9) \end{aligned}$$

Where we introduced notations $x = p/p_F(0)$, $y = p'/p_F(0)$.

We solved the system of equations numerically on a uniform grid in x containing 101 points. The integrals were approximated by trapezoidal formulas. The time evolution was described by an implicit, second-order, two-layer scheme. We solved the implicit difference system using a successive-approximation method.

The time dependence of the bubble density computed in this way and used in the numerical simulations is described well by the formula

$$\rho(t) = \frac{167.14}{1 + 0.3 \exp(t - 5.5)}. \quad (10)$$

3.3. Results of neutrino transport simulation

The results of our numerical solution presented in Figs. 2-5 for two cases: in the first (Figs. 2, 3), we

used formula (8) for the function $\gamma(x, t)$, and, in the second (Figs. 4, 5), we used formula (9).

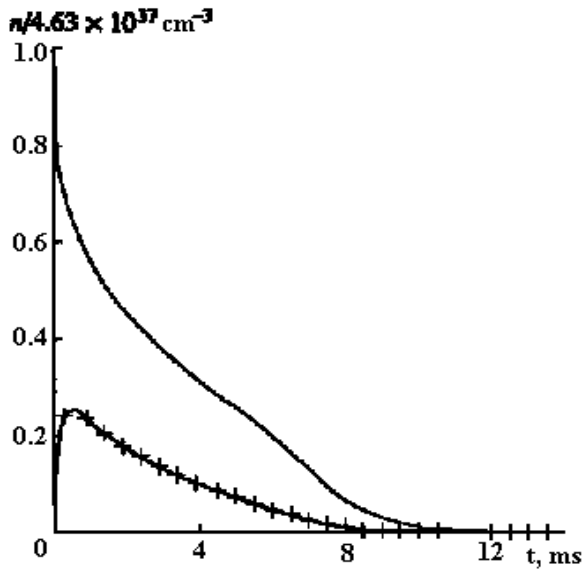


Figure 2: Time dependence of the number density of neutrinos (marked curve) and electrons (unmarked curve).

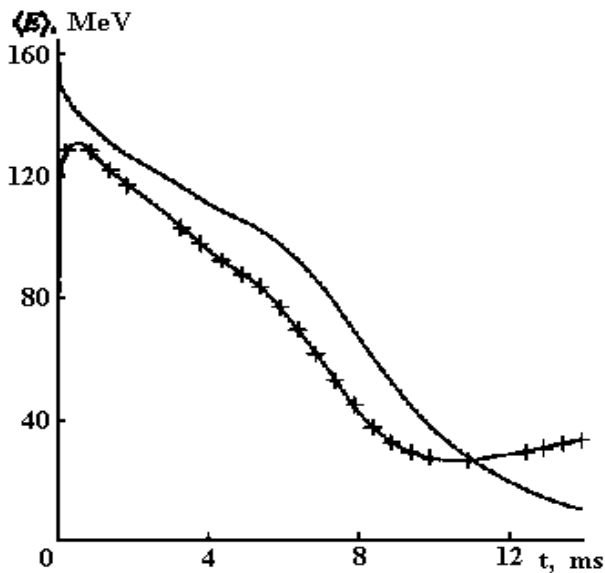


Figure 3: Time dependence of the average energies of the neutrinos (marked curve) and electrons (unmarked curve).

The neutrino distribution function outside the specified region was taken to be zero in both cases. The number of neutrinos emitted per unit volume per unit time in an interval dp is given in our model by the formula

$$dI(p, t) = \frac{4\pi c}{d(t)[1 + \gamma(p, t)](2\pi\hbar)^3} [f(p, t) - f_g(p, p_g)] p^2 dp = n_e(0)I(x, t)dx. \quad (11)$$

Although the difference between the two cases from the viewpoint of physical conditions seems negligible, the results of the numerical simulations are radically different. In the first case, the bubble is optically thin to the neutrino radiation from the very onset of the process. The emission maximum corresponds to time $t \approx 0.5 \text{ ms}$, which is roughly equal to the characteristic time for the action of the source. The transparency of the bubble results from the substantial decrease in neutrino scattering due to the factor $(1 - f)$ in (8), when the neutrino distribution function is close to a Fermi step function.

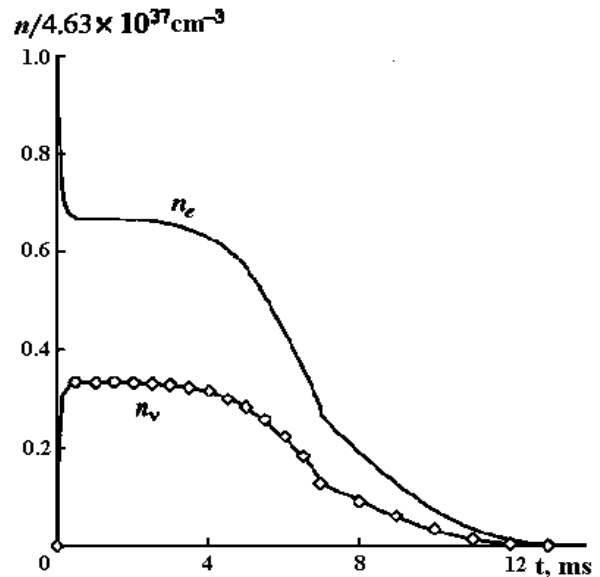


Figure 4: Time dependence of the number density of neutrinos (marked curve) and electrons (unmarked curve).

However, under real conditions, the distribution function can be considerably different from a Fermi step distribution, for example, due to the heating of the electron component by neutrino scattering processes. Since the model we have used cannot be applied to the case of non-zero temperature of the medium, we simulated the influence of non-degeneracy of the neutrino distribution on the emission by neglecting the suppression factor $(1 - f)$ when describing scattering by nuclei. Since the neutrino energy remains virtually unchanged during scattering by nuclei (as compared to scattering by electrons), this should not affect the evolution of the neutrino distribution in

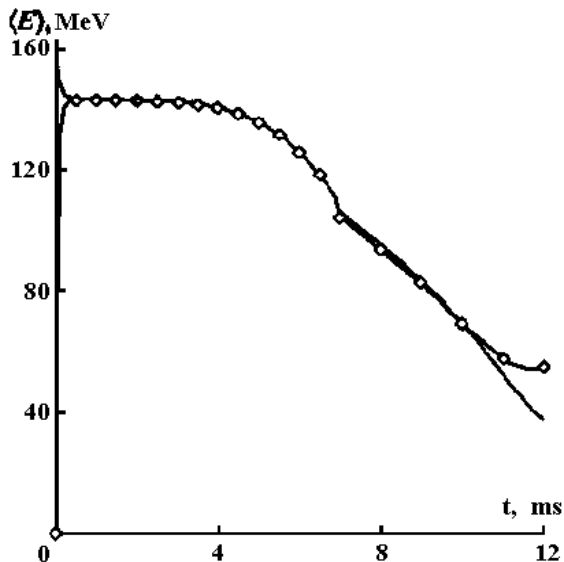


Figure 5: Time dependence of the average energies of the neutrinos (marked curve) and electrons (unmarked curve).

momentum space, and should change only the optical depth of the boundary [see (9)].

Indeed, in this case, appreciable neutrino radiation appears only after $t \approx 10 \text{ ms}$, and reaches its maximum at $t \approx 12 \text{ ms}$. In accordance with (10), such times correspond to densities that are two orders of magnitude lower than the initial density. Therefore, in the second case, the bubble becomes optically thin to neutrinos only after it rises to the upper layers of the supernova core, which are characterized by considerably lower density. At earlier times, the rising bubble acts as an opaque neutrino trap. In this case (Fig. 5), the mean energies of the neutrino and electron components are equal from $t \approx 0.5 \text{ ms}$ (the characteristic time required for production of the neutrino component by beta processes) to $t \approx 10 \text{ ms}$ (when the medium becomes optically thin). In the first case (Fig. 3), the average neutrino energy is less than the average electron energy, due to the emission of some of the neutrinos before the onset of the stage of "classical" transparency. Later, the mean neutrino energy exceeds the mean electron energy in both cases, since the degradation of neutrinos in νe processes is substantially decreased, while the Fermi energy of the electrons (and, consequently, their average energy) continues to decrease as the bubble expands.

3.4. Estimates of neutrino radiation

At the initial time, the mass of matter with excess entropy ($s_{max} = 2.5$) is $0.07M_{\odot}$. After 3.5 ms , $0.02M_{\odot}$ of this material approaches the boundary of the neutrino-sphere, where the density is $\rho =$

10^{11} g/cm^3 , and becomes transparent to the neutrinos there. The density of these neutrinos is comparable to the density of electrons with mean energy $E \sim 60 \text{ MeV}$. In this case, the intensity of the neutrino emission can be estimated as

$$L = (0.04M_{\odot} \times E) / (\mu m_n \times 3.5 \times 10^{-3}) \sim 4 \times 10^{54} \text{ erg/s},$$

Fraction of energy absorbed by matter per gram in the shock wave from this neutrino radiation is

$$\frac{d\epsilon}{dt} \sim L \sigma n_1 / \rho R^2 = 0.97 \times 10^{27} \text{ erg g}^{-1} \text{ s}^{-1},$$

for typical parameters $\rho = 10^8 \text{ g/cm}^3$, and $R = 10^7 \text{ cm}$. This is much more than the neutrino losses from the shock front: $d\epsilon_{\nu}/dt \sim 6 \times 10^{22} \text{ erg g}^{-1} \text{ s}^{-1}$ (reference [20]); i.e., the large-scale convection could support a diverging shock wave, leading to the ejection of the supernova envelope.

4. DISCUSSION AND CONCLUSIONS

The mechanism we have considered here is based on the development of large-scale hydro-dynamical instability inside a rotating protoneutron star, and has several advantages over previous models, because it can provide a rapid (over a time $\sim 10^{-2} \text{ s}$) emission of high-energy neutrinos, which can give the required boost to the energy of the shock. Observations of the central region of SN 1987A testify to the presence of two large-scale ejections, in good agreement with our model incorporating the effects of rotation [21]. In addition, the motion of the bubbles along the rotation axis will be accompanied by strong mixing and the intense formation of ^{56}Ni , which has been observed during the ejection of supernova shells. Since a large fraction of the evolution of the bubbles occurs at densities $\rho > 10^{12} \text{ g/cm}^3$, where neutrinos move in matter in a diffusion regime, there is no need to take into account the effects of neutrino transport on the development of the large-scale instability. As a bubble approaches the neutrinosphere ($\rho < 10^{12} \text{ g/cm}^3$), these effects become appreciable and lead to changes in the energy and spectrum of the escaping neutrinos.

References

- [1] Birrows, A., Hayes, J., and Fryxell, B.A., *Astrophys. J.*, 1995, vol. 450, p. 830.
- [2] Wilson, J.R. and Mayle, R.W., *Phys. Rep.*, 1993, vol. 227, p. 97.
- [3] Janka, H.-Th. and Muller, E., *Astron. Astrophys.*, 1996, vol. 306, p. 167.
- [4] Mezzacappa, A., Calder, A.C., and Bruenn, S.W., et al., *Astrophys. J.*, 1998, vol. 495, p. 911.

- [5] Imshennik, V.S., Pis'ma Astron. Zh., 1992, vol. 18, p. 489.
- [6] Aksenov, A.G., and Imshennik, V.S., Pis'ma Astron. Zh., 1994, vol. 20, p. 32.
- [7] Bisnovaty-Kogan, G.S., Astron. Zh., 1970, vol. 47, p. 813.
- [8] Ardelyan, N.V., Bisnovaty-Kogan, G.S., and Moiseenko, S.G., Usp. Fiz. Nauk., 1997, vol. 167, p. 11.
- [9] Chechetkin, V.M., Ustyugov, S.D., Gorbunov, A.A., and Polezhaev, V.I., Pis'ma Astron. Zh., 1997, vol. 23, p. 34.
- [10] Zueva, N.M., Mikhailova, M.S., and Solov'ev, L.S., Preprint of IPM AN SSSR, Moscow, 1976, no. 65.
- [11] Gerlakh, N.I., Zueva, N.M., and Solov'ev, L.S., Preprint of IPM AN SSSR, Moscow, 1975, no. 96.
- [12] Chandrasekhar, S., Lebovitz, Norman, R., Astrophysical Journal, 1963, vol. 138, p. 185
- [13] Lattimer, J.M., and Swest, F. D., Nucl. Phys. A, 1991, vol. 535, p. 331.
- [14] Yee, H. C., Klopfer, G. H., Montagne, J. L., JCP, 1990, vol. 88 p.31.
- [15] Shu, C. W., Osher, S., JCP, 1988, vol. 77, p.439.
- [16] Andrianov, A. N., Efimkin, K. N., Levashov, V. Y., Shishkova, I. N., Lecture Notes in Computer Science, v.2073, July, 2001.
- [17] Hachisu, K., Astrophys. J., Suppl. Ser., 1986, vol. 62, p. 461.
- [18] Sazhin, M.V., Ustyugov, S.D., and Chechetkin, V.M., Pis'ma ZhÉTF, 1996, vol. 64, p. 817.
- [19] Suslin, V. M., Ustyugov, S. D., and Churkina, G. P., Preprint No. 70, IPM im. M.V. Keldysha RAN (Keldysh Institute of Applied Mathematics, Russian Academy of Sciences, Moscow, 1998).
- [20] Fowler, W., and Hoyle, F., Neutrino Processes and Pair Formation in Massive Stars and Supernovae, Chicago, 1965.
- [21] NASA Press Release, *STScI-PR-97-03*.